Machining and heat treatment as post-processing strategies for Ni-superalloys structures fabricated using direct energy deposition

Careri, Francesco; Imbrogno, Stano; Umbrello, Domenico; Attallah, Moataz M.; Outeiro, José; Batista, António C.

DOI:
10.1016/j.jmapro.2020.11.024

Document Version
Peer reviewed version

Citation for published version (Harvard):
Careri, F, Imbrogno, S, Umbrello, D, Attallah, MM, Outeiro, J & Batista, AC 2021, 'Machining and heat treatment as post-processing strategies for Ni-superalloys structures fabricated using direct energy deposition', *Journal of Manufacturing Processes*, vol. 61, pp. 236-244. https://doi.org/10.1016/j.jmapro.2020.11.024

Machining and Heat Treatment as Post-Processing Strategies for Ni-Superalloys Structures Fabricated using Direct Energy Deposition

Francesco Careri[a, b], Stano Imbrogno[b,*], Domenico Umbrello[a], Moataz M. Attallah[b], José Outeiro[c], António C. Batista[d]

[a] *Department of Mechanical, Energy and Management Engineering, University of Calabria, Rende, CS 87036, Italy*

[b] *School of Metallurgy and Materials, University of Birmingham, Birmingham B15 2TT, UK*

[c] *Arts et Metiers Institute of Technology, LABOMAP, HESAM University, Rue Porte de Paris, F-71250 Cluny, France*

[d] *Univ Coimbra, CFisUC, Department of Physics, P-3004-516 Coimbra, Portugal*

*Corresponding author: s.imbrogno@bham.ac.uk, Tel.: +447882267415.

Abstract

The aim of this study is to determine the most suitable post-processing routines to enhance the surface integrity of components produced with Inconel 718 superalloy by additive manufacturing. The components were fabricated by Direct Energy Deposition (DED) followed by two typical post-processing methods: machining and heat treatment. The effect of the post-processing sequence (machining + heat treatment or heat treatment + machining) and the corresponding effects on the surface integrity of these components were investigated in terms of surface finishing, microstructure, micro-hardness and residual stresses. Finally, suitable solutions in terms of additive manufacturing - post-process operations have been reported.

Keywords: Machining; Additive Manufacturing; Surface integrity

1. Introduction

Additive Manufacturing (AM) offers a new technique to manufacture complex parts. During the last decade, AM has attracted the interest of relevant industrial areas such as aerospace, automotive and medical, thanks to its flexibility and potentiality to create near-net-shape components using innovative layer-by-layer manufacturing technology. [1, 2]. Amongst all the AM techniques, Direct Energy Deposition (DED) is considered the most promising for performing repair actions on high mechanical performance components e.g. turbine blades or blisks as well as producing parts with very complex thin shapes [3]. This process uses a thermal source, usually a laser or electron beam, to melt the metal powders blown thorough the nozzle with the superficial part of the substrate or the previous layer deposited [4]. In contrast, the parts produced by DED result in a very poor surface quality (high surface roughness) as well as not reaching the tolerance required. Therefore, the parts generally require further post-processes (subtractive operations) in order to match the high accuracy and surface quality required in the standards.

The Nickel-based superalloy Inconel 718 is known as a difficult-to-cut material because of its high strength at high temperatures, high reaction with tool materials and low thermal diffusivity [5]. More often, components produced with Inconel 718 require some specific heat treatments in order to achieve the mechanical properties and microstructural characteristics required, especially if produced by DED or other AM techniques [6]. Furthermore, these components demonstrate extraordinary mechanical properties after the heat treatments at the expense of machinability which is drastically compromised. For this reason, different studies have been conducted in order to identify the best combination of cutting parameters to machine the Inconel 718 [5-7]. However, most of the research carried out aimed to assess the machinability of the Inconel 718 in wrought or cast condition, whilst the machinability of the parts produced by DED or by further laser metal deposition processes is still not clear. Generally, the usual manufacturing procedure applied by industries, is to deposit the

material by the DED process. This is also known as hybrid additive manufacturing. The component is then heat treated and subsequently machined in order to achieve the final shape and the desired surface quality.

The present work aims to study and propose different industrial strategies to customise and achieve the required quality depending on the application of the components produced by AM techniques. In particular, three different hybrid additive manufacturing routines combined with heat treatments are investigated on Inconel 718 and machinability and surface integrity are also assessed. Microstructure, micro-hardness, and residual stresses resulting from the manufacturing processes are investigated in order to analyse the effects of the various manufacturing routines on the final quality of the produced part.

2. Material and methods

The material used in this research was the Nickel-based superalloy Inconel 718, provided as metal powder with a particle size varying from 45 to 106 µm particularly suitable for the DED process. The cylindrical bars (120mm length and 33mm diameter) were produced with a 5 axis CNC machine equipped with a TruDisk 4002 disk laser with a wavelength of 1030 nm (Fig. 2(a)). The AM process parameters were laser power of 400 W, scan speed of 275 mm/min and powder flow rate 9.8 g/min. The scan strategy is showed in Fig. 2(b). It is important to highlight that the process parameters set were obtained by a previous optimisation procedure which consisted of producing small cubes of 20mm x 20mm x 8mm for relative density and defects analyses. The combination of laser power, scan speed and powder flow rate selected, allowed parts with a relative density higher than 99% and free defects in the bulk cross sections to be obtained.

Firstly, the optimisation process parameters were carried out which investigated the porosity rate when three levels of power (300W – 400W – 500W) and three levels of scan speed (200mm/min – 275mm/min – 350mm/min) were used. Fig. 1(b) shows a picture of one of the small cubes produced

and the microstructure analysis of the cross section. It can be noted that when increasing the scan speed without changing the power, the pores significantly increase, especially when the power is not high enough to completely melt the material. In particular, high porosity and some lack of fusion were observed as shown in Fig. 1(d). The lowest level of pores was observed when the power was set to 400W and the scan speed to 275mm/min. These parameters represent the optimal combination and, therefore, were subsequently used to produce the cylindrical bars.

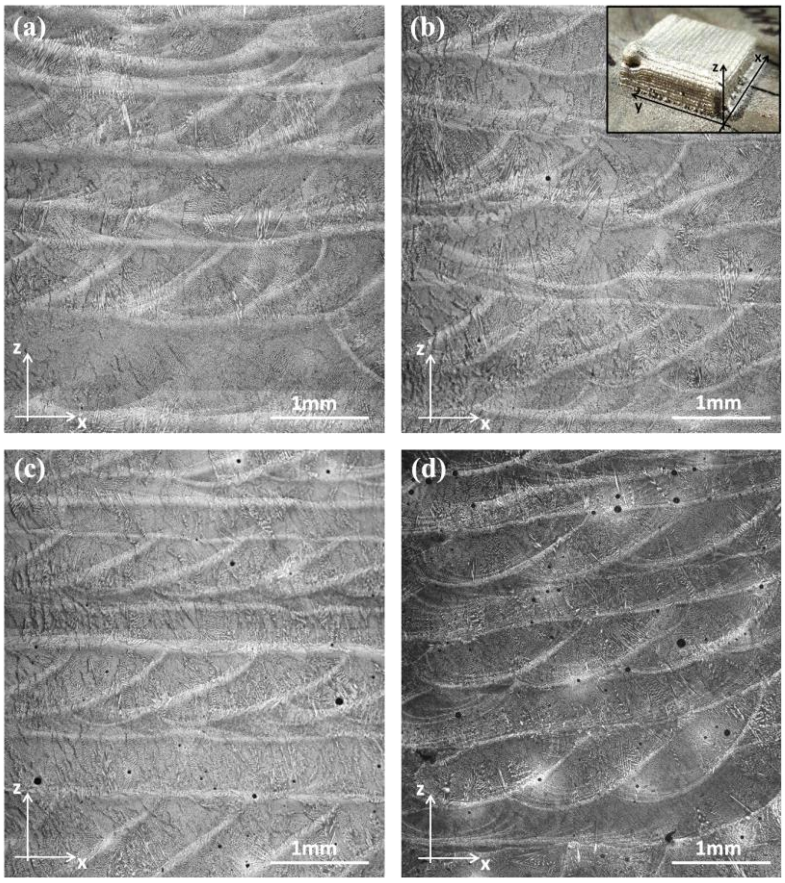

Fig. 1. Microstructure observed on the cross section; (a) 400W – 275mm/min; (b) 400W – 350mm/min; (c) 300W – 275mm/min; (d) 300W – 350mm/min.

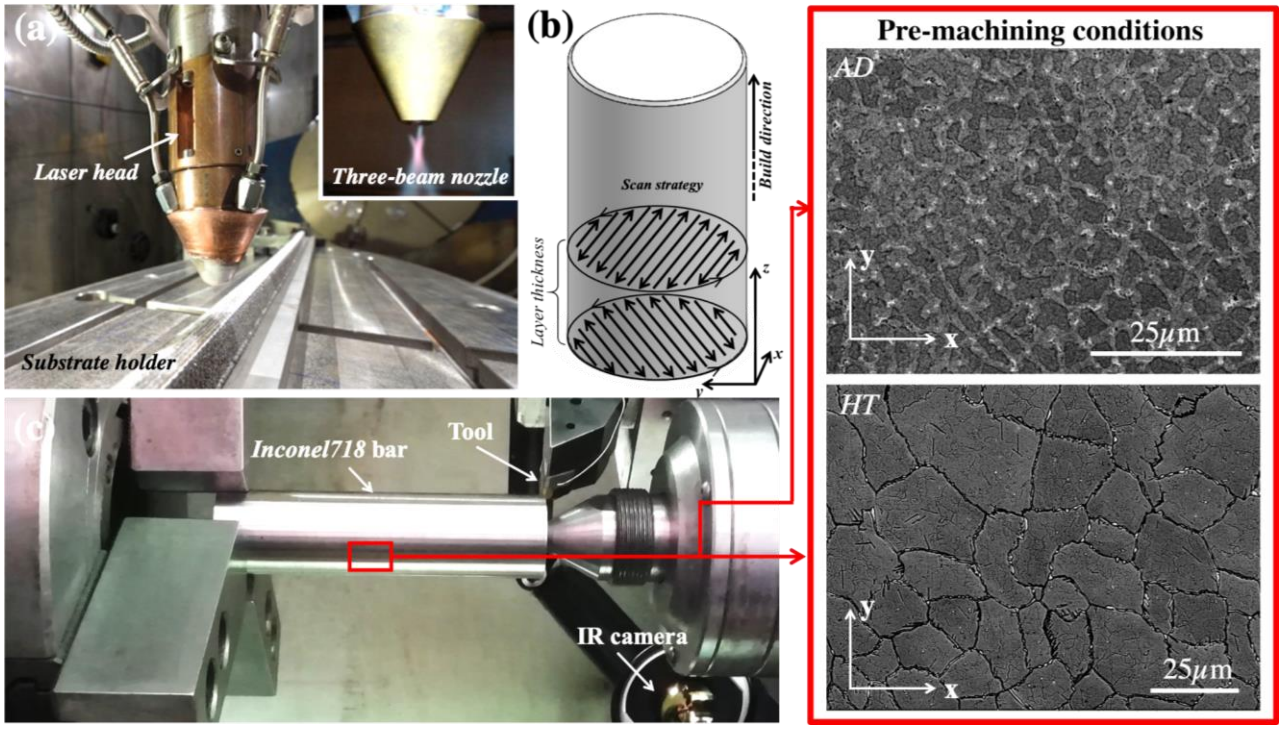

Fig. 2. (a) DED set-up; (b) schematic representation of the scan strategy used to build by DED; (c) machining set-up, microstructural features (cross section) of the samples as deposited (AD), after heat treatment (HT).

The powder was spread into the melt pool by a three-beam nozzle while the argon was shielding the pool to avoid oxidation phenomena. The focus of the laser was set to get a beam spot of approximately 1 mm while the stand-off distance was set equal to 10 mm. With this configuration, the auto compensation of the material deposited was triggered and this allowed a good deposition rate and high geometrical accuracy to be had [8]. It is very important to achieve an accurate set of stand-off distance and laser focus distance in order to avoid declining of side surfaces, unevenness and high roughness especially on the top surface as well as non-uniform layer thickness. The DED process produces parts with low surface quality with surface roughness commonly higher than 30 μm [9], as well as poor mechanical properties when missing out the strengthening phases needed when using Inconel 718). Therefore, post-processes treatments such as machining to improve the surface quality and heat treatment to enhance the mechanical properties were carried out. The cylindrical specimens were turned on a 2 axis CNC lathe under dry cutting conditions as the most representative case for hybrid additive manufacturing since no lubricants are used due to the presence of the laser. The

cutting speed was based on three levels (70, 90 and 120m/min), the feed rate was based on two levels (0.1 and 0.2mm/rev) whilst the depth of cut was kept constant at (0.5mm). The aforementioned cutting parameters are usually recommended for machining Nickel-based superalloys as suggested by the tool maker Sandvik® when a tool holder DDJNR 2525M 15 and tool DNMG 15 06 12-SMR S05F are used. The heat treatments selected for the Inconel 718 were recommended by the SAE AMS 5583D [10]. The heat treatment consisted of three steps:

i. Homogenisation treatment, to transform the dendritic in an equiaxed microstructure (1093±14°C for 2h and air cooling).
ii. Solution treatment, to dissolve (mostly) the Laves phase (968±14°C for 1h and air cooling).
iii. Double Ageing treatment, to allow the formation of the γ' and the γ'' phases responsible for the strengthening of the material (718±8°C for 8 h, cool it down to 621±8°C and hold for 8h, air cooling to room temperature).

In order to understand the effects of the different post-processes on the overall final quality of the produced parts, a combination of heat-treatment and machining steps and vice versa was investigated. In detail, the case studies are identified as: as deposited (AD), that is the material as produced by DED without any post-heat treatment; heat treated (HT) that is the material after the 3-steps heat treatment; double aged (DA), where the material was subjected only to the double ageing step. The machining (M) operation is also identified as another manufacturing step. Therefore, the three manufacturing routes studied are:

- AD+M: DED Manufacturing process followed by Machining process.
- AD+HT+M: DED Manufacturing process followed by Heat Treatment process (steps: i, ii, iii) followed by Machining process.
- AD+M+DA: DED Manufacturing process followed by Machining process followed by Double Ageing heat treatment process (step: iii).

The case AD+M+HT was not considered since, after the entire HT, some detrimental oxidation phenomena were observed on the surface and within a region of 30-50μm beneath the machined

surface. As highlighted by the literature, DED technology produces parts characterised by very poor surface quality, therefore they always require post-process operations, such as machining. This hybrid manufacturing approach allows the designed tolerances and geometric requirements to be achieved as well as enhancing the surface quality. Generally, the Hybrid Additive Manufacturing machine is characterised by two main steps: the deposition and subsequently machining or alternate strategies depending on the complexity of the part. It is clear that the adding or omission of these steps affects the properties (especially on the surface) of the finished part.

IN718, when processed by AM, always requires the heat treatment due to the low mechanical properties (the strengthening phases are missing) and the anisotropic behaviour (columnar dendritic microstructure). This alloy is also known as difficult-to-cut material. Therefore, this work needs to investigate and to characterise the machinability and the surface quality when the hybrid AM, and the heat treatment are coupled in different orders. As a result, the AD + M strategy, as well as the AD + M + DA strategy, would be more advantageous for the companies that operate in this market area, although sometimes the AD + HT + M could be a preferred strategy for example if the machine is not equipped with a hybrid AM hardware.

The machinability was assessed in terms of the cutting forces (cutting and thrust components) while the thermal gradient (frontal surface of the chip) was evaluated by an infrared (IR) camera. Preliminary calibration of the IR camera emissivity (0.5) was carried out by matching the temperature registered via thermocouple on a small sample heated on a hot surface.

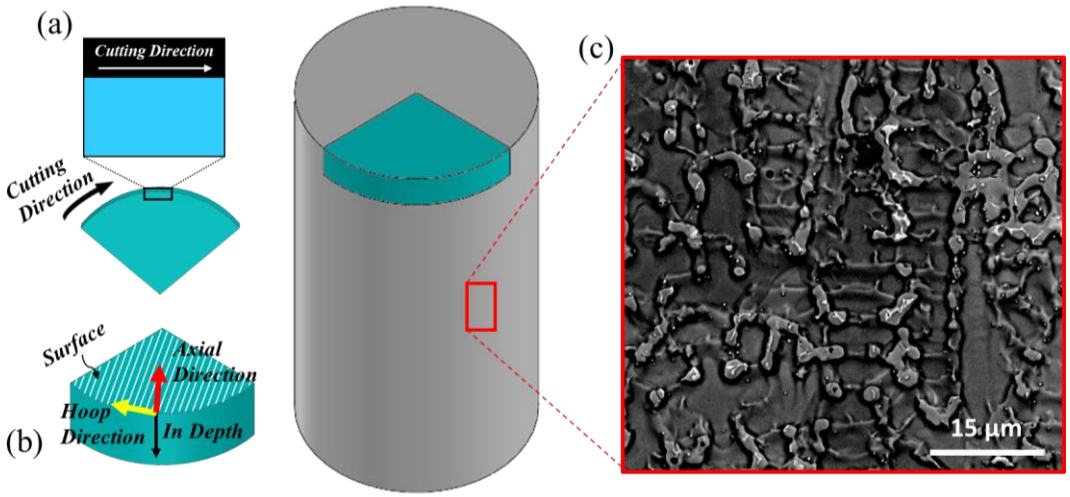

Fig. 3. Schematisation of a cross section of the sample for (a) microstructural and (b) residual stresses analysis. (c) microstructure of the as deposited material (cross section).

The surface quality after the post-processes were evaluated in terms of surface roughness (S_a) by a non-contact 3D confocal profilometer. The micro-hardness ($HV_{0.025}$) on the surface and beneath the machined part was measured on the polished cross section of the samples. Subsequently, the samples were etched through electrolytic etching (H_3PO_4 with a voltage of 6V and a time of 10s) to reveal the microstructure. The microstructural features and the alterations were assessed by means of Scanning Electron Microscopy (SEM) and Electron Backscatter Diffraction (EBSD), to examine the cross section of small samples collected from the bars as shown in Fig. 3(a). Finally, the residual stresses (RS) were analysed in the surface and subsurface of the samples using an X-ray diffraction technique [11]. X-ray Mn-K_α radiation was used to determine elastic strains in the {311} diffraction planes ($2\theta \approx 152°$) of the crystallographic structure of the Inconel 718 alloy, using 22° ψ angles in the range ±44°. Residual stresses were determined in the direction of the primary motion (hoop) and in the direction of the feed motion (axial), as reported in Fig. 3(b).

3. Results and Discussion

3.1 Forces and temperatures in machining

Fig. 4 shows the measured cutting and thrust forces as well as the chip temperature during the cutting process. As expected, the machinability of the AD+HT+M material was lower than the AD+M, since the precipitation strengthening phases made the material harder and therefore difficult to manufacture by machining processes. In general, both the cutting and thrust forces decreased when the cutting speed increased due to the effect of the increased thermal gradient. The Inconel 718 in particular, has a low thermal conductivity that drastically compromises the heat dissipation rate through the chip during the machining process, resulting in a higher thermal gradient and accumulation of heat within the cutting zone. Consequently, a higher accumulation of heat within the cutting zone led to a thermal softening effect on the material behaviour during the machining process. Moreover, higher forces when the AD+HT+M material was machined were obtained by increasing the feed rate.

In contrast, the AD+M showed lower cutting force when cutting speeds of 70 and 90 m/min (f=0.1mm/rev) were used whilst a cutting speed of 120m/min triggered wear affecting the tool tip and resulting in higher force. More significant differences were observed when the feed was set to 0.2mm/rev but it is interesting to note that there are significant differences between the HT and the AD materials. The AD+M parts showed a better machinability compared to the AD+HT+M where the cutting forces were lower than 40%-50% and the thrust force was lower than 80%. This result suggests that the AD+M has a higher ductility which is also suggested by the lower heat accumulated within the cutting zone. In addition, the maximum chip temperature is lower during the machining of the AD+M samples compared with the AD+HT. Consequently, the expected tool life when machining AD+M samples is likely to be higher than that achievable when machining the AD+HT+M.

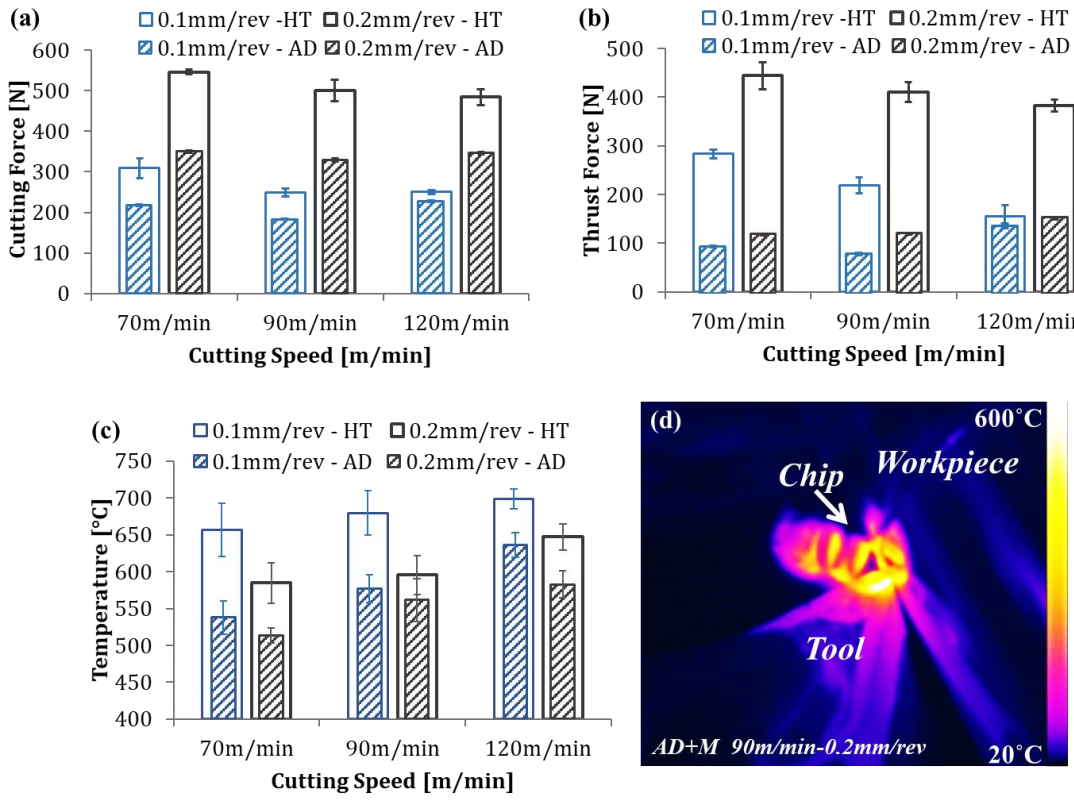

Fig. 4. Main variables of the machining process. (a) cutting force; (b) thrust force; (c) maximum temperature; (d) thermal field of the cutting zone acquired by the infrared camera.

3.2 Surface Roughness

The surface roughness in terms of S_a is shown in Fig. 5. The average value of the as deposited samples depends on the DED process parameters It is known that, usually, the surface roughness decreases with the increasing of the laser power and it increases with the increasing of the scan speed. In this study, the process parameters used were already optimised to achieve a high density of the part produced, therefore the surface roughness is due to the combination of the parameters set.

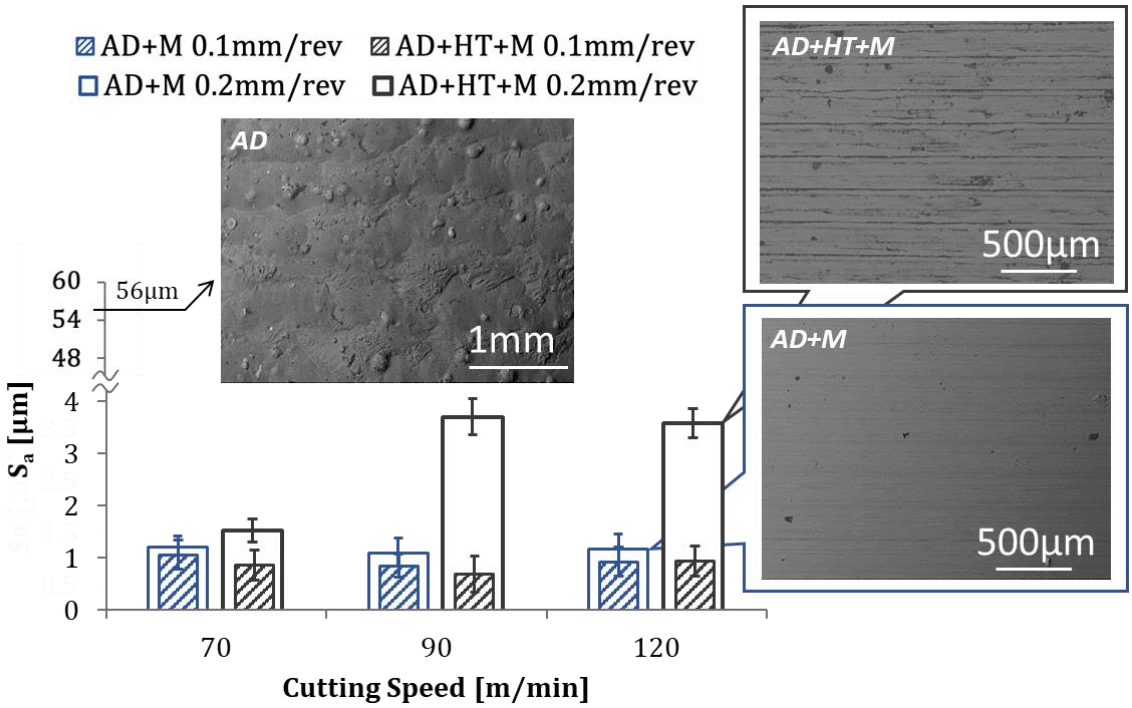

Fig. 5. S_a with different post-process parameters and heat treatments.

The average S_a of 56µm was measured on the bars after the DED process and the value is similar to others reported in literature for parts produced by the DED process. Subsequently, depending on the post-process routine investigated, the S_a were evaluated, and the values were compared with the 56µm initially measured. The combination of the feed rate (higher value) and the heat treatment played an important role in the surface quality. While the lower feed rate allowed a low value of S_a to be achieved, the HT and the higher feed rate led to a critical change in the surface quality.

This effect is also amplified when higher cutting speeds are used during the AD+HT+M. Similar observations with different values of feed rate are highlighted in the work of Javadi et al. [12]. Although the surface roughness is much lower than the initial state (56 µm), the S_a of the AD+M is better than the AD+HT+M. The AD material, which was not heat treated, showed better ductility as also confirmed by the lower value of the cutting forces. The micrograph reported in Fig. 5 for the AD+M shows a smoother surface compared with that observed on the AD+HT+M samples where the tool wear clearly affected the surface quality resulting in higher surface roughness.

A smooth machined surface suggests that the material has a better ductility and machinability achievable when the HT is not performed. The improved results in terms of surface quality suggest, therefore, a reduced wear phenomenon of the tool since the micrograph does not show the typical signs of deterioration on the machined surface e.g. smearing. Moreover, it is important to highlight that generally under dry machining the surface roughness tends to decrease with increasing of cutting speed [13] but, in this study, the higher feed rate applied to the heat treated material triggered tool wear that catastrophically affected the surface roughness when the cutting speed was increased. On the contrary, when the AD material is directly machined, the surface roughness variation is almost negligible therefore the possibility of using higher removal material rate parameters does not negatively affect the surface quality.

3.3 Microstructure

Fig. 6 shows the microstructure of the cross section near the machined surface when the most critical cutting parameters were used. The impact of the combination between machining and heat treatment on the material microstructure is clearly visible. The deformation behaviour as well as the affected layer (AL), in particular, are different (Fig. 6(a), (b) and (c)). The deformation mechanisms due to the plastic deformation caused by the tool during the machining process are different depending on the material conditions. The AD+HT+M samples always showed the presence of slip bands beneath the machined surface and their formation increased with the intensity of the plastic deformation from the bulk up to the machined surface. As also highlighted by Imbrogno et al. (2018) by numerical simulations, the region with a high concentration of slip bands induced by machining on Waspaloy suggested a high concentration of dislocations and therefore high plastic deformation accumulation (strain-hardening) due to localised shear effects [14]. This result is also presented by Fig. 6(e), the Kernel average misorientation (KAM) maps that represent a qualitative indicator of the dislocations density, the local misorientation maps and the strain amongst the grains [15] and the EBSD.

Sometimes, the slip bands accumulation forms a place with cell structures for the formation of new grains due to the double-cross slip mechanism. However, the EBSD analysis did not show any dynamically recrystallized grains but only a lower indexing due to the high plastic deformation accumulated by the material. On the contrary, the AD+M subsurface was characterised by a different deformation mechanism highlighted by the intense smeared material typical of the ductile materials. Moreover, the more brittle Laves phase regions were trapped within the Al and were dragged following the cutting direction suggesting that the γ matrix was softer than the segregated regions (Fig. 6(c)). The KAM map and the EBSD suggested a high accumulation of energy caused by plastic strain and dislocations and the grains were mainly deformed through the preferential direction induced by the tool during the machining process (Fig. 6(d)). Consequently, it is clear that the material behaviour during the machining process is changing between ductile and more inclined to accommodate plastic deformation to harder with the formation of slip bands.

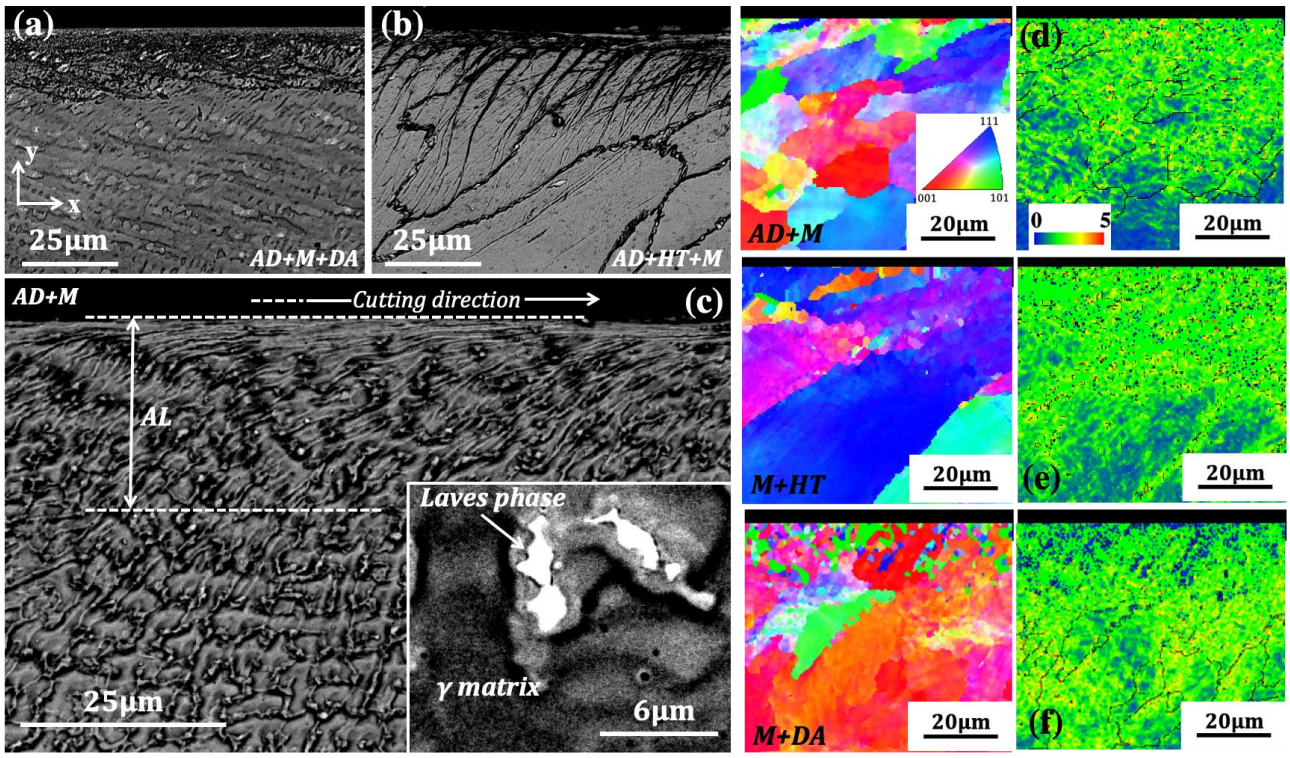

Fig. 6. Cross section of the machined bars (120m/min - 0.2mm/rev). (a) AD+M+DA; (b) AD+HT+M; (c) AD+M; (d), (e) and (f) EBSD and KAM map of the affected layer.

The AD+M+DA showed interesting results for concerning the effect of the heat treatment on the microstructure. As suggested by the KAM map, the small blue regions represented a relaxed condition, a gradual reduction of residual strains and dislocation densities, and this is also due to a very small recrystallized area highlighted by the EBSD (Fig. 6(f)) due to the heat treatment. Although, micrographs of the other samples are not reported, the thickness of AL increased when the cutting speed and feed rate increased and the grains, dendritic in AD+M, AD+M+DA and equiaxed in AD+HT+M, are mainly deformed following the cutting direction. Moreover, the intense plastic deformation induced by 90m/min and 120m/min (f=0.2mm/rev), led to the formation of a very thin plastically deformed layer (Fig. 6(a), (b) and (c)) while the microstructure is characterised by high angle boundaries and similar results were also observed in other published works [14, 16, 17]. In all the samples analysed, the accumulated strain was uniformly distributed, therefore no accumulation regions such as cracks, or grain boundaries were highlighted.

3.4 Hardness and residual stresses

In materials such as Inconel 718, hardness and residual stresses are two important factors to consider due to its engineering application fields [18]. Fig. 7 shows plots of the micro-hardness measured from 10 μm beneath the machined surface through the radial direction inside the samples. The hardness near the surface reached high values and it then rapidly decreased to the values measured within the bulk area (AD=260$HV_{0.025}$, HT=430$HV_{0.025}$, DA=428$HV_{0.025}$). As reported in Fig. 6(a) and (d), higher cutting speeds and feed rates led to the accumulation of residual strain and dislocation density that consequently resulted in an increase of the hardness of the material on the surface and beneath the machined area. Moreover, increasing the cutting speed and feed rate increased the AL thickness (Fig. 7), as also confirmed by the SEM analysis (Fig. 6). However, the AL thickness obtained by the

hardness profile was higher than that observed by the SEM analysis due to the strain hardening induced by the machining in the grains beneath the plastically deformed region.

The deepest AL thickness was obtained after the manufacturing route AD+HT+M (Fig. 7(b)). In this case, the cutting parameters did not cause significant effects in hardness changes as were observed in the AD+M samples (Fig. 7(a)). The AD+M samples showed the highest variation of hardness and the effect of the feed rate and cutting speed is clearly observable. The most significant effect in hardness variation is related to the feed rate changes rather than the cutting speed. Moreover, the higher hardness variation of more than $100HV_{0.025}$ when a cutting speed of 120m/min and a feed rate of 0.2mm/rev are used compared to the variation on the AD+M+DA and AD+HT+M, highlights the higher ductility of the material before any heat treatment. Concerning the AD+HT+M, the bulk material showed higher hardness due to the strengthening phase produced by the HT and the highest variation induced by the machining process is approximately $63HV_{0.025}$ suggesting a lower ductility of the material since less strain hardening was accumulated during the machining process.

The most interesting results are represented in Fig. 7(c) (AD+M+DA). The hardness measured was comparable to the AD+HT+M and the variation beneath the machine surface was still evident. The DA treatment enhanced the hardness at high values regardless of the cutting parameters used. Moreover, the possibility of reaching a comparable hardness value on the surface and sub-surface area of the material after the DA treatment suggests that it is possible to perform the machining step before the heat treatment process, thus taking advantage of the better machinability of the material. Although the AD+HT+M showed comparable results with the AD+M+DA, the machinability of the material after the HT step is drastically compromised as is also highlighted by the cutting forces and the temperatures. Although, the DA treatment led to a very small recrystallised area within the 5-6μm layer beneath the machined surface characterised by reduced accumulated strain hardening (blue spots showed by the KAM map Fig. 6(f)) the major contribution to the hardness was mainly represented by the strengthening phase formation.

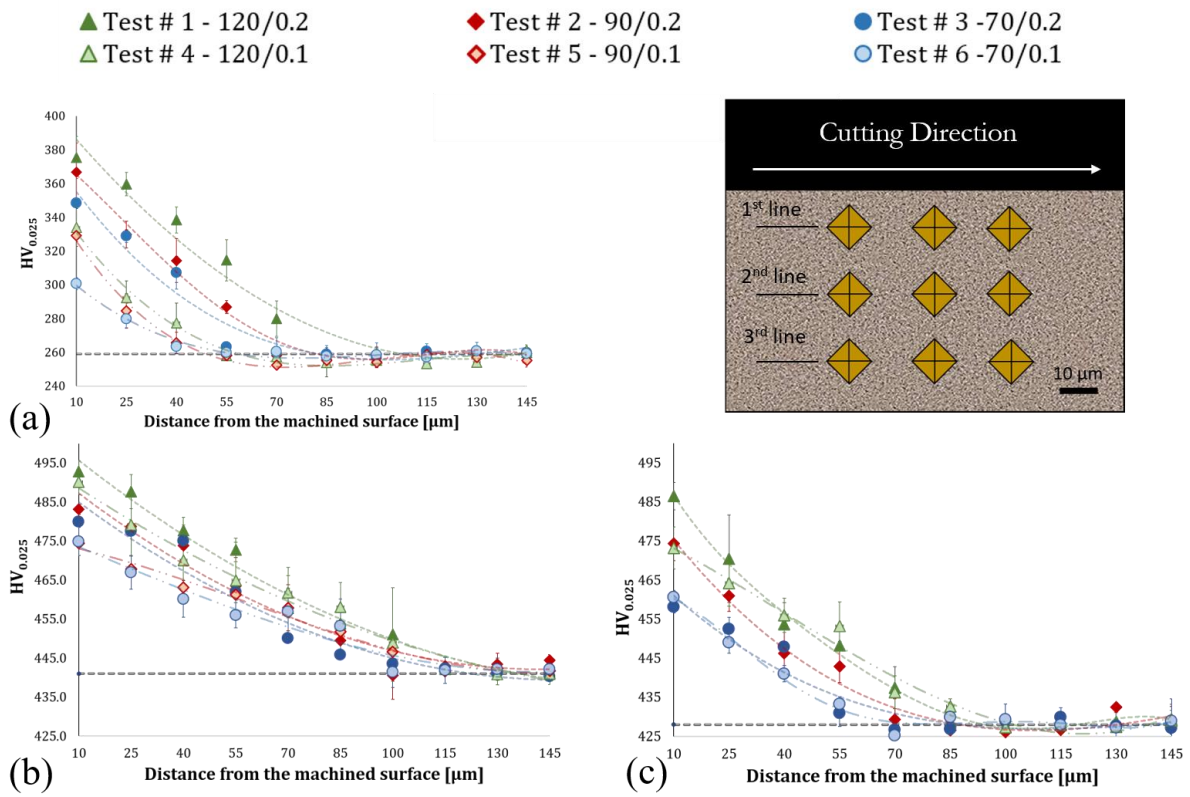

Fig. 7. Micro-hardness distribution. (a) AD+M; (b) AD+HT+M and (c) AD+M+DA.

Fig. 8 shows the residual stress measured on the machined surface. The hoop direction is oriented as the cutting speed while the axial direction is oriented as the feed motion. The residual stresses in the hoop direction are generally higher than those in the axial direction due to the higher plastic deformation caused by the tool during the machining process. The AD+M always showed higher and tensile residual stresses compared to the other experimental tests investigated and this is a consequence of the absence of heat treatment that usually contributes to the relaxation of stresses Focusing on the AD+HT+M samples, the residual stresses detected were mainly tensile, although increasing the feed rate, more compressive stresses in the axial direction were observed due to the higher plastic deformation caused by the tool.

The AD+M+DA showed the lowest residual tensile or compressive stresses. This result is mainly due to the heat treatment performed at the end of the manufacturing process that effectively reduced the residual stresses. It is interesting to observe two important phenomena. Firstly, when the cutting speed

is increased, especially with a higher feed rate, the residual stresses are mainly compressive except with a cutting speed of 70m/min and feed rate of 0.1mm/rev. Secondly, comparing the AD+M with the AD+M+DA, the double ageing heat treatment helps to transform the tensile residual stresses in compressive residual stresses.

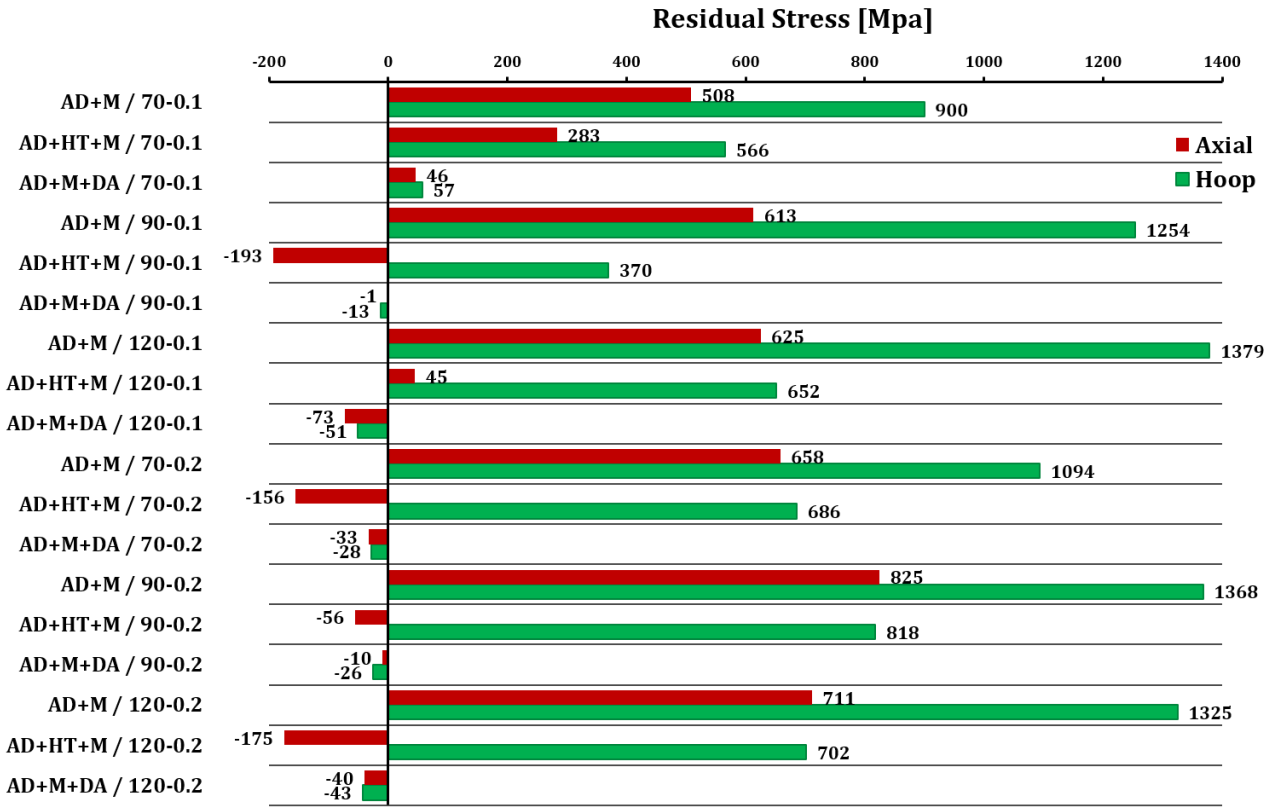

Fig. 8. Residual stresses measured on sample surfaces.

The residual stresses distributions were also analysed in depth within the material during the most critical cutting process of 120m/min and 0.2mm/rev and the results are reported in Fig. 9. It is evident that the distribution of the residual stresses in the hoop and axial directions is quite different. The hoop residual stresses near the surface are more tensile in comparison with the axial direction, although, the hoop stresses decreased rapidly from tensile to compressive area beneath the machined surface. Moreover, the thickness of the layer affected by tensile stresses is greater for the AD+M, approximately 70µm in the hoop direction and 20µm in the axial direction, compared to the

AD+HT+M, approximately 40μm in the hoop direction and absent in the axial direction. This is mainly related to the ductility of the material when machined before the heat treatment.

While the AD+M+DA samples showed compressive residual stresses both in the hoop and axial directions, it appears that the double ageing treatment had positive effects on the entire area deformed by the passage of the cutting tool as also reported by Barros et al. [19]. The AD+M shows the presence of initial high tensile residual stress that slightly become compressive according to the axial direction whilst tending to zero in the hoop direction. Shah et al. [20] observed the presence of mainly tensile residual stresses on small components manufactured by DED. It is possible, therefore, that the AD bars already contained tensile residual stresses due to the process of additive manufacturing. The values observed in Figs. 8 and 9 represent the superimposition of the effect on the residual stresses distribution by the additive manufacturing and machining process.

It is also interesting to highlight that the AD+HT+M showed mainly compressive stresses of almost -600MPa in the axial direction as shown in Fig. 9(a) and a transition between tensile and compressive in the axial direction. In this case, the effect of the heat treatment enhances the formation of compressive residual stress mainly in the axial direction. The AD+M+DA shows the most interesting results as the double ageing treatment, in particular, allowed the achievement of compressive or absent residual stresses distributions after the machining operation (Figs. 9(a) and 9(b)).

Although fatigue life was not investigated in this study, the hardening and the residual stresses induced by machining process have a significant impact on the fatigue behaviour of the material [21]. Therefore, the residual stresses and hardness distribution induced by the manufacturing strategy AD+M+DA can potentially produce beneficial effects in terms of fatigue life on the produced parts, as well as the fatigue crack propagation threshold due to the high degree of work hardening [22].

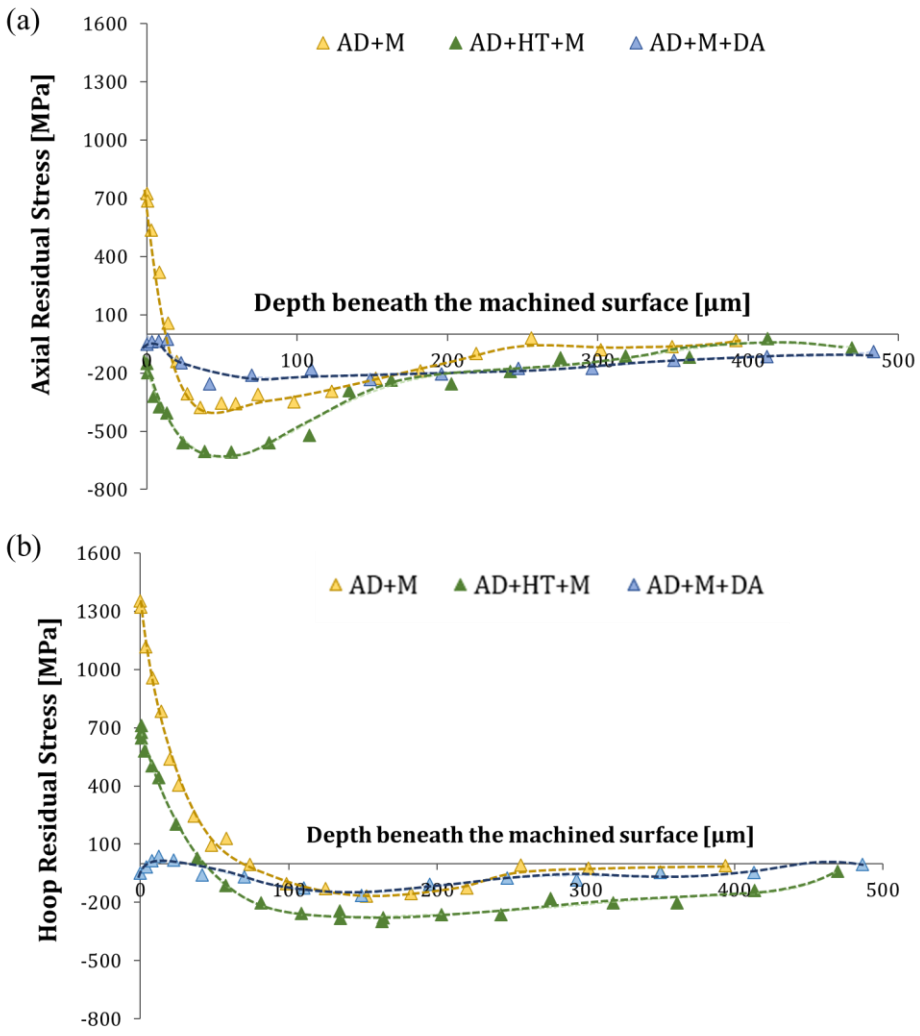

Fig. 9. Subsurface RSs distribution (120m/min and 0.2mm/rev) a) axial residual stress; b) hoop residual stress.

4. Conclusions

The effects of heat treatments and the machining operation, with the different cutting parameters, on the surface integrity of Inconel 718 produced by additive manufacturing were investigated. The experimental outcomes reported in this paper demonstrate the influence of the three hybrid manufacturing routes (AD+M, AD+HT+M and AD+M+DA) applied to Inconel 718. The three strategies analysed were selected to evaluate and compare strategies conventionally used (AD + HT + M) with strategies that could be more advantageous in terms of production times, and therefore of production cost within Hybrid Manufacturing processes. As a result, the experimental outcomes

suggest that the strategy AD+M showed the best machinability conditions due to the higher ductility of the material related to the absence of the strengthening phase. Low surface roughness and high surface hardness were also observed. However, the residual stresses were predominantly tensile, especially at the surface, mainly due to the combined effects of the DED and the machining process. On the contrary, the AD+HT+M represented the poorest strategy regarding the machinability as the heat treatment led to the strengthening phases formation, although the samples showed an increase of surface hardness and more compressive residual stresses were induced in the axial direction. Finally, the AD+M+DA represented a better manufacturing strategy since the component was machined before the DA treatment providing improved machinability and taking advantage of the higher ductility of the material (low surface roughness). Subsequently, the double ageing treatment allowed the transformation of the residual stresses leading to compressive or negligible residual stresses as well as higher hardness.

Acknowledgements

The authors would like to acknowledge the European research project that funded this research. The project belongs to Horizon 2020 research and innovation programme Novel ALL-IN-ONE machines, robots and systems for affordable, worldwide and lifetime Distributed 3D hybrid manufacturing and repair operations (Project ID: 723795).

References

[1] Kakinuma Y, Mori M, Oda Y, Mori T, Kashihara M, Hansel A, Fujishima M. Influence of Metal Powder Characteristics on Product Quality with Directed Energy Deposition of Inconel 625. CIRP Annals - Manufacturing Technology 2016; 65/1:209-212.

[2] Schmidt M, Merklein M, Bourell D, Dimitrov D, Hausotte T, Wegener K, et al. Laser based additive manufacturing in industry and academia. CIRP Annals - Manufacturing Technology 2017; 66/2:561-583.

[3] ISO / ASTM52900-15. Standard Terminology for Additive Manufacturing – General Principles – Terminology. ASTM International, West Conshohocken, PA; 2015.

[4] Bourell D, Kruth JP, Leu M, Levy G, Rosen D, Beese AM, Clare A. Materials for additive manufacturing. CIRP Annals - Manufacturing Technology 2017; 66/2:659-681.

[5] Hosseini E, Popovich VA. A review of mechanical properties of additively manufactured Inconel 718, Additive Manufacturing. 2019; 30:100877.

[6] M'Saoubi R, Axinte D, Soo SL, Nobel C, Attia H, Kappmeyer G, Engin S, Sim WM. High performance cutting of advanced aerospace alloys and composite materials. CIRP Annals - Manufacturing Technology 2015; 64/2:557-580.

[7] Soo SL, Khan SA, Aspinwall DK, Harden P, Mantle AL, Kappmeyer G, Pearson D, M'Saoubi R. High speed turning of Inconel 718 using PVD-coated PCBN tools. CIRP Annals - Manufacturing Technology 2016; 65/1:89-92.

[8] Zhu G, Li D, Zhang A, Pi G, Tang Y. The influence of standoff variations on the forming accuracy in laser direct metal deposition. Rapid Prototyping Journal 2011; 17/2:98-106.

[9] Mahamood MR. Laser Metal Deposition Process of Metals, Alloys, and Composite Materials. 1st ed. Springer; 2018.

[10] SAE International, 2006, Nickel Alloy, Corrosion and Heat-Resistant, Seamless Tubing 72Ni-15.5Cr-0.95Cb-2.5Ti-0.70Al-7.0Fe Vacuum Melted Solution Heat Treated, Precipitation Hardenable to 170 ksi (1172 Mpa) Tensile Strength (AMS5583D), AMS F Corrosion Heat Resistant Alloys Committee.

[11] Noyan IC, Cohen JB. Residual Stress – Measurement by Diffraction and Interpretation. 1st ed. New York: Springen; 1987.

[12] Javadi H, Jomaa W, Songmene V, Brochu M, Bocher P. Inconel 718 Superalloy Controlled Surface Integrity for Fatigue Produced by Precision Turning. International Journal of Precision Engineering and Manufacturing 2019; 20/8:1297-1310.

[13] Devillez A, Le Coz G, Dominiak S, Dudzinski D. Dry machining of Inconel 718, workpiece surface integrity. Journal of Materials Processing Technology 2011; 211/10:1590-1598.

[14] Imbrogno S, Rinaldi S, Umbrello S, Filice L, Franchi R, Del Prete A, A physically based constitutive model for predicting the surface integrity in machining of Waspaloy, Materials and Design 2018; 152:140-155.

[15] Gussev MN, Leonard KJ. In situ SEM-EBSD analysis of plastic deformation mechanism in neutron-irradiated austenitic steel. Journal of Nuclear Materials 2019; 517:45-56.

[16] Deng SQ, Godfrey A, Liu W, Hansen N. A gradient nanostructure generated in pure copper by platen friction sliding deformation. Scripta Materialia 2016; 117:41-45.

[17] Puerta Velásquez JD, Tidu A, Bolle B, Chevrier P, Fundenberger JJ. Sub-surface and surface analysis of high speed machined Ti-6Al-4V alloy. Materials Science and Engineering A 2010; 527/10:2572-2578.

[18] Pusavec F, Hamdi H, Kopac J, Jawahir IS. Surface integrity in cryogenic machining of nichel based alloy-Inconel718. Journal of Materials Processing Technology 2011; 211/4:773-78.

[19] Barros R, Silva FJG, Gouveia RM, Saboori A, Marchese G, Biamino S, Salmi A, Atzeni E. Laser Powder Bed Fusion of Inconel 718: Residual Stress Analysis Before and After Heat Treatment. Metals 2019; 4:1290.

[20] Shah K, Haq IU, Shah SA, Khan FU, Khan MT, Khan S. Experimental study of direct laser deposition of Ti-6Al-4V and Inconel 718 by using pulsed parameters. The Scientific World Journal 2014; 2014: 841549.

[21] Sasahara H. The effect on fatigue life of residual stress and surface hardness resulting from different cutting conditions of 0.45%C steel. International Journal of Machine Tools & Manufacture 2005; 45:131-136.

[22] Hua Y, Zhanqiang L. Effects of cutting parameters and tool nose radius on surface roughness and work hardening during dry turning Inconel 718. The International Journal of Advanced Machining Technology 2018; 96:5-8.